Positional stability as the light emission limit in sonoluminescence with sulfuric acid

Raúl Urteaga, Damián H. Dellavale, Gabriela F. Puente, and Fabián J. Bonetto
Laboratorio de Cavitación y Biotecnología, 8400 - Instituto Balseiro/Centro Atómico Bariloche - RN, Argentina
(Received 21 June 2007; published 29 November 2007)

We studied a single bubble sonoluminescence system consisting of an argon bubble in a sulfuric acid aq. solution. We experimentally determined the relevant variables of the system. We also measured the bubble position, extent of the bubble orbits, and light intensity as a function of acoustic pressure for different argon concentrations. We find that the Bjerknes force is responsible for the bubble mean position and this imposes a limitation in the maximum acoustic pressure that can be applied to the bubble. The Rayleigh-Taylor instability does not play a role in this system and, at a given gas concentration, the SL intensity depends more on the bubble time of collapse than any other investigated parameter.

DOI: 10.1103/PhysRevE.76.056317 PACS number(s): 78.60.Mq

I. INTRODUCTION

The single bubble sonoluminescence (SBSL) phenomenon is an impressive example of energy concentration. It is produced when an acoustically trapped bubble collapses violently enough to heat the gas inside and produce a light pulse emission. SBSL has been largely studied since its discovery [1,2]. A lot of working fluids have been tested but water has prevailed as the one that produces the most intense flash.

A change in this scenario was produced when Flannigan and Suslick [3] produced single bubble sonoluminescence (SBSL) using a sulfuric acid 85% wt. aq. solution as the working fluid achieving more than a hundred fold increases in light emissions compared to a near freezing water system.

Hopkins *et al.* [4] reported an increase of the order of 200 times for the 67 mbar xenon in sulfuric acid solution with respect to the near freezing 67 mbar xenon in pure water. They also found a strong dependence of the light emissions with the amount of dissolved noble gases. Nevertheless, the spatial stability of the bubble in sulfuric acid solutions is much more complex than in water. An SL bubble in sulfuric acid describes pseudo-orbits which amplitude and frequency vary with the acoustic pressure [5]. Moreover, when the acoustic pressure is increased enough, the overall movement of the bubble is shifted from the center to the walls of the resonator. A further increase in the acoustic pressure even can develop a discrete lattice of trapped bubbles [6], but cannot produce the extinction of the bubble, conversely to the SBSL behavior in water systems.

In water systems, the existence of a complex high harmonics pressure field has been demonstrated to play a crucial role in the spatial stability of the bubble [7]. This acoustic pressure field is the result of the excitation of high-order normal modes of the resonator by pressure pulses generated by the bubble collapses.

In this paper, we study the spatial stability of the sulfuric acid system in a wide range of parameter values. We changed the acoustic pressure from the onset of the sonoluminescence to the value where the bubble was next to the resonator wall.

We explored the concentration of the dissolved argon from concentrations where we failed to detect luminescence ($c_\infty/c_0<0.01$, where c_∞ and c_0 are the gas concentration far away from the bubble and the saturation, respectively) to gas concentrations where the bubble orbits were too large to produce the measurements reported here ($c_\infty/c_0>0.2$).

We compared the experimental data with the positions of the different instabilities in a calculated phase diagram.

II. EXPERIMENT

The basic system was described in [8]. We mention here the major changes. Experiments were carried out in a quartz spherical resonator 89 mm in outer diameter containing an acid sulfuric 85% wt. aq. solution. The second spherical mode was excited, resulting in a resonant frequency of about 33.7 KHz. Argon was dissolved in the degassed solution and the mixture was transferred under vacuum to the closed resonator. The filling resonator port had a long and small in diameter teflon tube filled with the mixture that allowed pressure equalization with the atmosphere and at the same time prevented gas diffusion to the resonator during time scales of the experiment. The static pressure in the resonator was $P_\infty=0.925$ bar and the temperature was $T_\infty=23\ ^\circ$C. A bubble was seeded into the resonator either using a Nd:YAG 20 mJ 20 ns laser pulse focused to the resonator center or increasing the acoustic pressure to produce cavitation and then reducing the pressure to operating levels.

We measured the sonoluminescence intensity (SL), the time of collapse and the bubble position within the resonator as a function of the driving voltage from the onset of the SL to values where the bubble is located near to the resonator walls.

We measured the intensity of the light emissions with two independent systems. We used a system that consisted of a phototube in conjunction with a gated integrator/boxcar averager. We normally integrated 300 or 1000 SL pulses in each data point recorded. This system is practical when the bubble is near the center of the resonator. The second system used a CCD camera with an integration time of 300 ms. The camera was slightly defocused to prevent saturation and enhance the dynamical range. This camera also provides the information of the position of the bubble. Since the mayor displacement of the bubble is in general about a radius, the position of the camera was selected to be perpendicular to this radius. The position of the bubble in the resonator was corrected by the refraction in the spherical resonator.

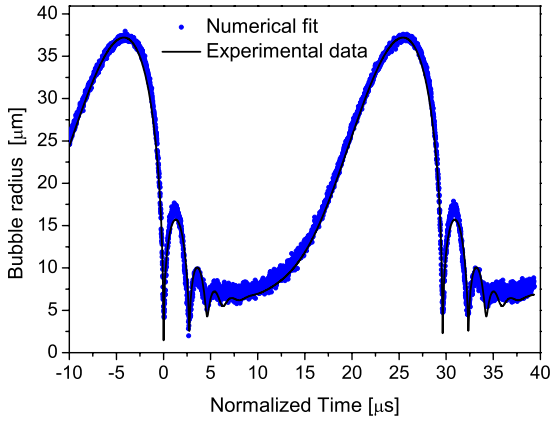

FIG. 1. (Color online) Bubble radius temporal evolution from Mie scattering. The data points (blue online) are the photomultiplier signal (30 averaged traces) with the background signal removed and converted to a signal proportional to the bubble radius. The solid curve is the result of the model with fitted parameters $R_0 = (7.96 \pm 0.05)$ μm and $P_a = (1.33 \pm 0.05)$ atm following the procedure described in Ref. [8]. The time of collapse is 18.7 μs. The noble gas (argon) pressure head for this run was 16.5 mbar.

We measured the time of collapse defined as the time interval between the acoustic pressure zero crossing with negative slope and the sonoluminescence pulse arrival. The external microphone signal was low pass filtered and input to a lock-in which was referenced to the excitation frequency in order to obtain both the resonant frequency component of the microphone signal and the start for a timer (Stanford Research Systems SR620). The timer stop was obtained from a Dantec X57 photomultiplier signal amplified X25 using a 300 MHz amplifier (Stanford Research Systems SR145). A delay (Stanford Research Systems DG535) was used to control the timing of the gated integrator (GI), the GI window, and the arming of the timer.

To determine the bubble radius temporal evolution we use conventional Mie scattering techniques [9,10]. The obtained data was compared with a model described in [11] to determine all the quantities of interest. In the model, and due to the fact that the vapor pressure of the solution consists of water vapor we used the accommodation coefficient of water [12]. In particular, the combination of the experimental data with the model allowed us to obtain the acoustic pressure P_a and calibrate the microphone signal.

A set of measurements were performed in the low acoustic pressure range where the bubble is spatially stable and non-SL. Another series of measurements were made at high acoustic pressure to verify linearity of acoustic pressure with the microphone voltage signal. In the later case the traces were taken as single shot to prevent errors produced by the movement of the bubble.

III. RESULTS

Figure 1 shows both the measured and fitted bubble radius temporal evolution. The measured data points are the square root of the voltage trace obtained by averaging 30 oscilloscope traces from the photomultiplier. The fitting curve was obtained using the model described in [8]. The parameters R_0 and P_a minimize the square integral of the absolute error (least squares χ^2 method). The agreement between the experimental results and the model are excellent and of a similar quality as observed in water [9]. In particular, the timing and the relative amplitude of the rebounds are in very good agreement between experiment and model.

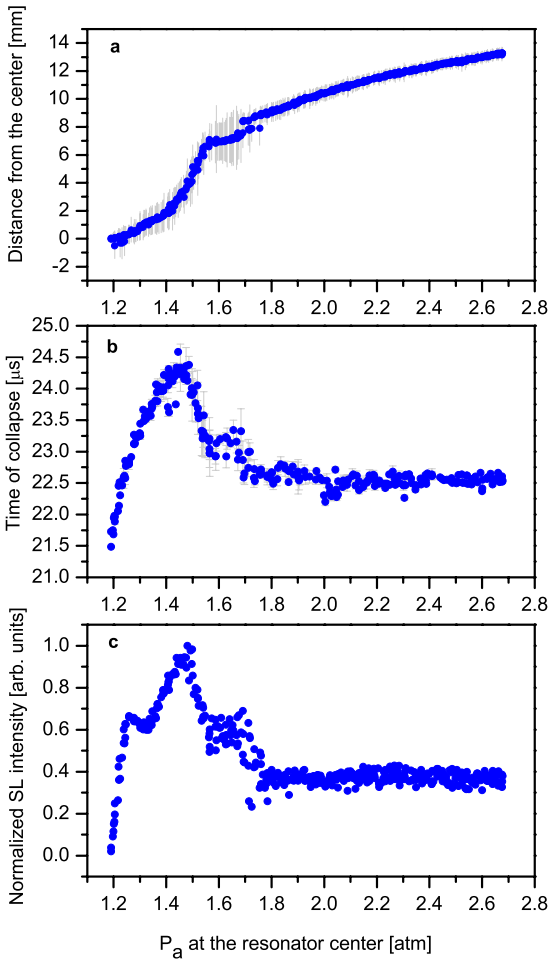

FIG. 2. (Color online) (a) Position of the bubble as a function of the acoustic pressure in the center of the resonator. The error bar in the figure shows the size of the orbit in the radial direction. (b) Time of collapse defined as the interval since the acoustic pressure zero crossing with negative slope to the sonoluminescence pulse arrival. The error bars are the standard deviation of five measurements at each point. (c) Normalized intensity of SL emission as measured by the CCD camera with 300 ms of integration time.

The concentration that results from the fit is $c_\infty/c_0 = 0.023$ whereas the liquid was in contact with argon at 16.5 mbar ($c_\infty/c_0 = 0.018$) previous to the transfer to the resonator. We computed the acoustic pressure with this well tested method for several experimental traces throughout the whole parameter space and in no case we obtained values higher than 1.8 bar for a sonoluminescent bubble.

Figure 2 shows the position of the bubble, the time of collapse and the SL intensity as a function of the acoustic pressure in the center of the resonator for a run with 30 mbar

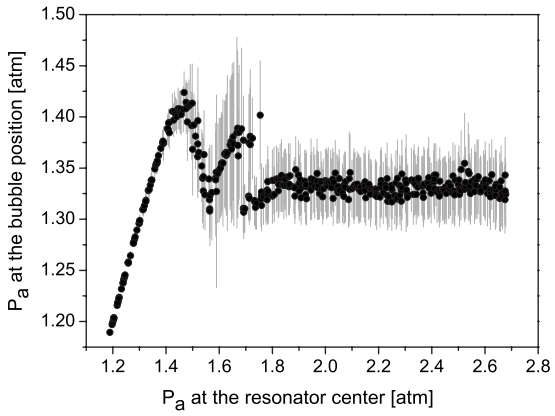

FIG. 3. Acoustic pressure at the bubble position as calculated by Eq. (1). The error bars shows the variation in acoustic pressure as a consequence of the movement of the bubble [error bars in Fig. 2(a)]. The absolute error from the calibration of the acoustic pressure is 0.05 atm almost constant in the overall range. This extra error is not shown for clearness.

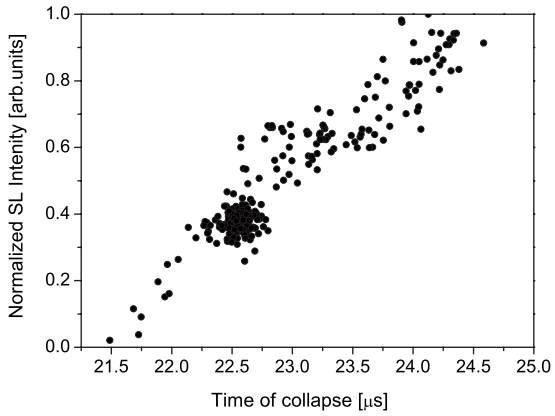

FIG. 4. Normalized SL intensity as a function of time of collapse. The relation is almost linear with a wider dispersion for high SL intensities.

argon pressure head. All the experimental points correspond to SL conditions. In Fig. 2(a) the error bars describes the size of the orbit in the radial direction. Since the working frequency in this experiment was about 33.7 KHz, the first pressure node was about 22 mm from the center (sound velocity 1480 m/s).

In Fig. 2(a) is possible to observe that the bubble moves away from the center monotonically at different velocities upon the acoustic pressure. For low acoustic pressures the bubble remains close to the center of the resonator. A rather fast increase of the distance is noticed between 1.4 and 1.7 atm. In this region the size of the orbit in the radial direction is maximum. For pressures higher than 1.7 atm the bubble continues moving to higher radius but with lower rates.

Figures 2(b) and 2(c) shows a similar structure. Both have a maximum at about 1.45 atm and remain almost constant for acoustic pressures higher than 1.8 atm. The major difference between Figs. 2(b) and 2(c) is a small kink at about 1.3 atm in the SL intensity that does not have a correlation on the time of collapse.

It is important to note that at the bubble position, the acoustic pressure is lower than in the center of the resonator. Assuming a spherical resonant mode, the ratio between them is given by the zero-order spherical Bessel function:

$$\frac{P_a(r)}{P_a(0)} = \frac{\sin\left(\frac{2\pi fr}{c}\right)}{\frac{2\pi fr}{c}}, \tag{1}$$

where r is the bubble position, f the frequency, and c the sound velocity in the liquid.

Taking this ratio into account, it is possible to calculate the pressure that the bubble experiences (P_a^b) as a function of the pressure in the resonator center (P_a^c). This computation is shown in Fig. 3.

In this figure we can see that the P_a^b increase almost linearly until about 1.4 atm. This behavior is consistent with the fact that the bubble remains approximately in the center for this range of pressure. The P_a^b shows a maximum at about 1.43 atm. Moreover, the maximum in P_a^b coincides with the maximum of SL intensity and time of collapse.

Between 1.4 atm and 1.7 atm, P_a^b shows a few oscillations and, for $P_a^c > 1.7$ atm, it reaches a constant value of about 1.33 atm. In this later region, a change in P_a^c results in a displacement of the bubble to a region in which the pressure that bubble experiences remains unchanged.

The similarity of Figs. 2(b) and 2(c), and Fig. 3 suggest a proportionality between the time of collapse, the acoustic pressure, and the SL intensity. This behavior is similar to that observed in water-SBSL. In Fig. 4 the SL intensity is plotted as a function of the time of collapse.

Figure 4 shows that the relation is almost linear except for a wider dispersion for high SL intensities. This suggests that if one can increase the time of collapse the SL fluence can be increased.

The acoustic pressure also shows a similar behavior but with more significant differences. This fact can be related with the existence of a complex acoustic field at higher frequencies than the fundamental.

In Fig. 5 we show the high frequency component of the microphone signal (US_{HF}). This US_{HF} is calculated as the rms value after the subtraction of the first harmonic.

The maximum value in this curve, reached at $P_a^c = 1.3$ atm, is about 10% of the first harmonic signal. The US_{HF} presents a rich structure and is formed by harmonics up to 15 times the fundamental (where the frequency response of the microphone decreases).

Two facts must be noticed in this figure. The first is that the overall value of US_{HF} decreases for high values of the acoustic pressure. The second is that this quantity is the only one of the measured variables that shows a similar behavior as the SL intensity at $P_a^c = 1.3$ atm [Fig. 2(c)]. This can be interpreted as evidence that the kink in the SL intensity is related to a modification in the dynamics of the bubble by the excitation with high frequency harmonics.

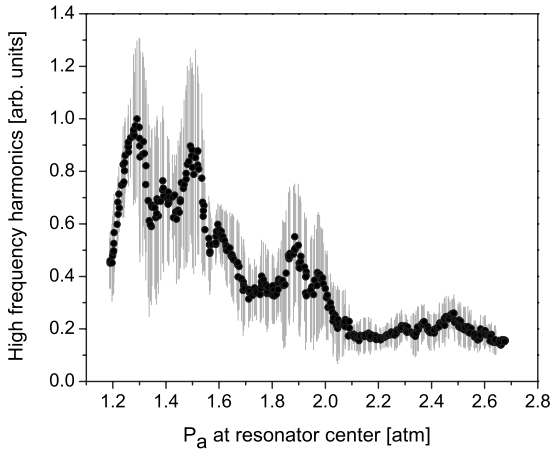

FIG. 5. Normalized high frequency component of the microphone signal. The value is an rms quantity obtained from the subtraction of the first harmonic to the complete signal. The curve is a moving average of five points and the error bar is obtained from the standard deviation of these five points.

IV. ANALYSIS

In this section we examine a simplified picture of the forces on the bubble with the aim of retain the most relevant component regarding the mean position of the bubble in the resonator. Neglecting the history forces, which are the origin of the bubble movement in quasiperiodic orbits [5], the total force on the bubble can be calculated as [13]

$$F_T = -V_{(t)}(\nabla P_{(t,r)} - \rho g\hat{z}) - \frac{1}{2}\rho\frac{d}{dt}[V_{(t)}u_r] - \frac{12\rho u_r^2 R_{(t)^2}}{\mathrm{Re}}, \tag{2}$$

where $V_{(t)}$ is the bubble volume, $P_{(t,r)}$ the acoustic pressure in the resonator, ρ the liquid density, g the gravity acceleration, u_r the relative velocity of the bubble respect to the liquid, R the radius of the bubble, and Re the Reynold number defined has $2\rho u_r R/\mu$.

As pointed out by Matula [13], the added mass force and drag [the two last terms in Eq. (2)], have a little effect on the mean position of the bubble. Furthermore, we neglect the buoyancy force taking into account that at the measured bubble positions $\nabla P >> \rho g$. Finally, the resultant force is the primary Bjerknes force.

We then calculate the primary Bjerknes force on the bubble in a phase diagram R0-Pa. We search the points where this force becomes zero.

The mean primary Bjerknes force (F_B) can be calculated by the following equation: [14–16]

$$F_B = \frac{4\pi}{3T}\int_0^T -\nabla P_{(t,r)} \cdot R_{(t)}^3 dt = 0, \tag{3}$$

where P is the acoustic pressure and T is the time period.

In Fig. 6 we show the fixed points in the phase diagram where Eq. (3) is satisfied according to the numerical model presented in [11]. In the same figure are included the parametric and Rayleigh-Taylor instabilities.

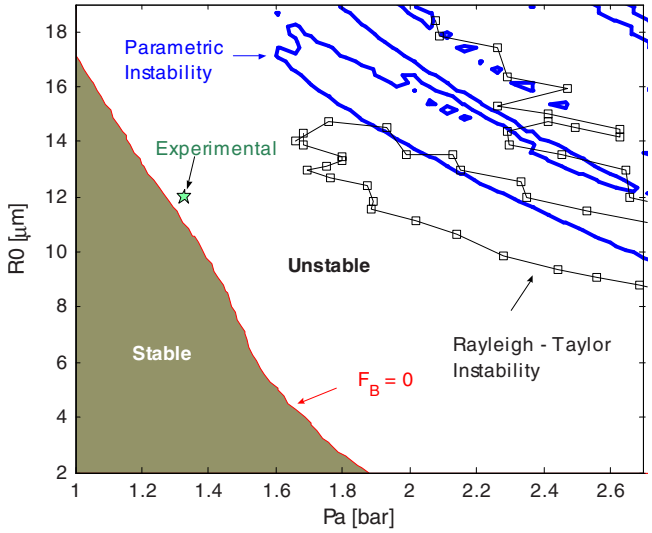

FIG. 6. (Color online) Phase space diagram of the fixed points. In the figure are included the zero primary Bjerknes force (F_B=0) (continuous red line), the parametric instability (doted blue line), and the Rayleigh-Taylor instability (continuous black line with squares). The star mark in the diagram show the position of the fixed point measured at the end of Figs. 2 and 3 (1.33 atm, 22.5 μs).

In the figure we place a star mark at the fixed point that was measured at the end of Figs. 2 and 3, i.e., at 1.33 atm and 22.5 μs. For this point corresponds a value of c_∞/c_0 =0.034, in accordance with the dissolved argon (30 mbar, c_∞/c_0=0.0326).

Typically, Eq. (3) is satisfied in two cases: When $\nabla \boldsymbol{P}$=0 (antinode of pressure) or when $\boldsymbol{R}$ is constant (node of pressure). The stability of these points is determined by the bubble size [14]. For bubbles smaller than the resonant size the antinode is stable and the node unstable. The opposite is true for bubbles bigger than the resonant size.

We want to point out that there is another condition in which Eq. (3) can also be satisfied. This condition arises when the dynamic of the bubble has the exact temporal evolution necessary to make the temporal integration equal to zero [15,16].

In the region labeled as stable in Fig. 6, the point where F_B=0 is at the pressure antinode, i.e., the resonator center. When the acoustic pressure is increased towards the unstable region, the dynamic of the bubble makes the integral in Eq. (3) to change of sign and F_B=0 occurs at the node of pressure (a spherical nodal surface of 22 mm radius in our case). However, when the bubble moves away from the center, the acoustic pressure at the bubble position decrease until F_B becomes zero again. For this reason, a new stable radial position is created which acoustic pressure is on the curve of the Fig. 6 labeled as "F_B=0."

Thus, if the acoustic pressure in the center is further increased, the only effect on the bubble is that the stable position lies on a higher radius, but the acoustic pressure remains constant, and in consequence, the complete dynamics of the bubble remains unchanged. In particular, the SL intensity and the time of collapse remain unchanged as observed at the end of Fig. 2.

It is worth noting that in Fig. 3 there are points where the acoustic pressure is higher than the final value of 1.33 atm. These points also have more intense SL emissions and higher values of time of collapse (Fig. 2). This fact can be addressed to the existence of high frequency harmonics in the sound field that modify mainly the values of the pressure gradient.

These modifications are more important respect to the pressure gradient of the fundamental mode at positions near of the resonator center where the later is low. The exact modification is quite complex since depends on the fraction of each harmonic and their phases. A correct choice of these parameters can extend the stable phase space of Fig. 6.

However, in the region where the high frequency harmonics are low and the pressure gradient of the fundamental mode is high, i.e., at bubble positions far away from the center, the preceding analysis will be correct.

V. SUMMARY AND CONCLUSIONS

When the acoustic pressure is increased the bubble moves away from the resonator center towards regions where the acoustic pressure intensity is a fraction of the acoustic pressure intensity in the resonator center. The Rayleigh-Plesset equation as a part of a complete model (as described in [8,11]) correctly represents the experimental data. The time of collapse for SBSL in sulfuric acid correlate linearly with the sonoluminescence fluence.

Taking into account the primary Bjerknes force only, we are able to explain the measured mean position of the bubble in the resonator as a function of the acoustic pressure. This simplified analysis predicts that the bubble moves away from the center when the acoustic pressure is increased. This occurs in order to maintain the pressure on the bubble at a constant value. We did not find any indication of the Rayleigh-Taylor instability to produce the bubble extinction.

The onset of the Rayleigh-Taylor instability is connected with the destruction of the bubble into fragments. This fact was never observed in the experiments. Moreover, the predicted position of the instability is quite distant from the experimentally determined points that are positioned in the stable region limit. The high viscosity in sulfuric prevent the occurrence of Rayleigh-Taylor instabilities.

The Bjerknes force is acting by moving the bubble from the resonator center but is not producing bubble extinction. This force operates as a limiting process that prevents the access to higher values of acoustic pressure and then to higher SL emissions.

Furthermore, this force is extremely sensitive to the existence of high frequency harmonics since it depends on the gradient of the pressure field. In fact, the high frequency acoustic field that bubble produces modifies the position and stability of the bubble itself.

Moreover, another harmonic in the driving force could be included to enhance the stability of the bubble and increase the range of acoustic pressures available.

ACKNOWLEDGMENTS

We acknowledge the technical support of Sebastian Eckardt and Daniel Mateos. G.F.P. is financed by Anpcyt/Secyt and RU by CONICET/CNEA. The partial support of Foncyt/Anpcyt/Secyt through Grant No. PICT 12-09848 is gratefully appreciated.

[1] D. F. Gaitan, L. A. Crum, C. C. Church, and R. A. Roy, J. Acoust. Soc. Am. **91**, 3166 (1992).
[2] M. P. Brenner, S. Hilgendfeldt, and D. Lohse, Rev. Mod. Phys. **74**, 425 (2002).
[3] D. J. Flannigan and K. S. Suslick, Nature (London) **434**, 52 (2005).
[4] S. D. Hopkins, S. J. Putterman, B. A. Kappus, K. S. Suslick, and C. G. Camara, Phys. Rev. Lett. **95**, 254301 (2005).
[5] R. Toegel, S. Luther, and D. Lohse, Phys. Rev. Lett. **96**, 114301 (2006).
[6] A. Troia, D. M. Ripa, and R. Spagnolo, Ultrason. Sonochem. **13**, 278 (2006).
[7] J. Holzfuss, M. Ruggeberg, and R. G. Holt, Phys. Rev. E **66**, 046630 (2002).
[8] G. F. Puente, R. Urteaga, and F. J. Bonetto, Phys. Rev. E **72**, 046305 (2005).
[9] B. P. Barber and S. J. Putterman, Phys. Rev. Lett. **69**, 3839 (1992).
[10] T. J. Matula, Philos. Trans. R. Soc. London, Ser. A **357**, 225 (1999).
[11] G. F. Puente, PabloGarcía-Martínez, and F. J. Bonetto, Phys. Rev. E **75**, 016314 (2007).
[12] G. F. Puente and F. J. Bonetto, Phys. Rev. E **71**, 056309 (2005).
[13] T. J. Matula, J. Acoust. Soc. Am. **114**, 775 (2003).
[14] T. G. Leighton, A. J. Walton, and M. J. W. Pickworth, Eur. J. Phys. **11**, 47 (1990).
[15] I. Akhatov, R. Mettin, C. D. Ohl, U. Parlitz, and W. Lauterborn, Phys. Rev. E **55**, 3747 (1997).
[16] T. J. Matula, S. M. Cordry, R. A. Roy, and L. A. Crum, J. Acoust. Soc. Am. **102**, 1522 (1997).